Electro-catalytic performance of 60%NiO/Ce$_{0.9}$Zr$_{0.1}$O$_2$ cermets as anodes of intermediate temperature solid oxide fuel cells

M.G. Zimicz [a,b], P. Núñez [c], J.C. Ruiz-Morales [c], D.G. Lamas [d], S.A. Larrondo [a,e,*]

[a] CINSO (Centro de Investigaciones en Sólidos), UNIDEF-CONICET, J.B. de La Salle N°4397, 1603 Villa Martelli, Pcia. de Buenos Aires, Argentina
[b] Instituto de Física del Sur – CONICET, Av. Alem N°1253, 8000 Bahía Blanca, Pcia. de Buenos Aires, Argentina
[c] Departamento de Química Inorgánica, Universidad de La Laguna, Av. Astrofísico Fco. Sánchez s/n (E-38206), La Laguna, Tenerife, Islas Canarias, Spain
[d] Laboratorio de Caracterización de Materiales, Facultad de Ingeniería, Universidad Nacional del Comahue, Buenos Aires 1400, 8300 Neuquén Capital, Pcia. de Neuquén, Argentina and CONICET, Argentina
[e] Departamento de Ingeniería Química, Facultad de Ingeniería, Universidad de Buenos Aires, Pabellón de Industrias, Ciudad Universitaria, 1428 Buenos Aires, Argentina

HIGHLIGHTS

- A New 60%NiO/Ce$_{0.9}$Zr$_{0.1}$O$_2$ (ZDC6) nanomaterial was proposed as anode of SOFCs.
- These anodes were successfully fixed onto SDC disks keeping their high porosity.
- Dual-chamber SOFCs with these anodes were fully characterized in pure H$_2$.
- The SOFCs exhibited good power densities of 75 mW cm^{-2} when operated at 650 °C.

ARTICLE INFO

ABSTRACT

This paper analyses the electrocatalytic performance of a 60%NiO/Ce$_{0.9}$Zr$_{0.1}$O$_2$ anode under reducing atmospheres, using a symmetric cell configuration, [anode/electrolyte/anode], with Samaria doped Ceria (SDC) as electrolyte. This anode exhibited excellent performance in H$_2$ atmosphere in comparison with conventional anode materials. A dual chamber solid oxide fuel cell with 60%NiO/Ce$_{0.9}$Zr$_{0.1}$O$_2$ anode, SDC electrolyte, and Pt cathode was constructed and tested under H$_2$ atmospheres at intermediate temperatures. Good values of power densities were obtained, indicating the good performance of 60%NiO/Ce$_{0.9}$Zr$_{0.1}$O$_2$ in the operating conditions.

1. Introduction

Solid Oxide Fuel Cells (SOFCs) have great potential in clean and sustainable production of energy. One of the goals to achieve, in order to make this technology economically competitive, is to reduce its operating temperature from 1000 °C to the 500–800 °C range. The main challenge is to develop new materials capable to sustain high electrocatalytic performance and minimal ohmic losses during operation at reduced temperatures. In this context,

anode materials have been a major focus of interest for many researchers. The anode material has to fulfil special requirements such as stable microstructure, high ionic and electronic conductivities and high catalytic activity at reduced temperatures [1]. Besides, when a SOFC is fuelled with hydrocarbons the anode material should be resistant to sulphur poisoning while avoiding carbon deposits formation. In recent years several excellent reviews in SOFC anodes, such as Cu–Ce/YSZ, Pd–CeO$_2$/YSZ [3], (La,Sr/Ca)(Ti,Sc/Nb/Cr)O$_{3\pm\delta}$, (La,Sr)(Cr,Ru)O$_3$, Niobium-doped-zirconia, gadolinia–terbia and samaria-doped-ceria [5], Sc$_2$O$_3$–Y$_2$O$_3$–ZrO$_2$–TiO$_2$, La$_{0.75}$Sr$_{0.25}$Cr$_{0.5}$Mn$_{0.5}$O$_{3-\delta}$ have been published [1–7].

CeO$_2$-based mixed oxides have received considerable attention in the formulation of anode materials for SOFCs. These materials exhibit ionic and electronic conductivity in reducing atmospheres, and excellent catalytic properties for the combustion of

* Corresponding author. Departamento de Ingeniería Química, Facultad de Ingeniería, Universidad de Buenos Aires, Pabellón de Industrias, Ciudad Universitaria, 1428 Buenos Aires, Argentina. Tel.: +54 11 47098158.
  E-mail addresses: susana@di.fcen.uba.ar, sushilarrondo@yahoo.com.ar (S.A. Larrondo).

hydrocarbons. It has been also reported that anodes based on ceria (CeO_2) are resistant to carbon deposition, making possible their use with direct feeding of dry hydrocarbons as fuels [8]. These facts positioned them as suitable candidates for anode formulation, especially for operation at intermediate temperatures with direct feeding of hydrocarbons.

Among CeO_2-based materials, Sm_2O_3 or Gd_2O_3-doped CeO_2 (denoted as SDC and GDC, respectively) have received great attention due to their high ionic conductivity below 650 °C ($\sim 0.3\ S\ cm^{-1}$) [9], and many important studies on these systems have been published in the last years [4,10–15]. It is important to note that, in reducing atmospheres, total conductivity of ceria-based ceramics increases due to an increase of the electronic contribution. Besides, ceria doped with zirconia (ZrO_2) appears to be an attractive alternative for anode applications, especially at intermediate temperatures, seldom explored in the literature. Doping with ZrO_2 increases the thermal resistance, diminishes the grain growth with temperature and improves the reducibility of both surface and bulk ceria sites [16]. Ceria–Zirconia solid solutions exhibited high catalytic activity [16–18] and some studies regarding the influence of synthesis conditions on their morphology, reducibility and catalytic activity have been published recently [19–21].

Even though the ceria-based materials exhibit mixed ionic and electronic conductivities, their electronic conductivities are not high enough to achieve a good anode performance. Therefore, composite ceramic-metal materials ('cermets') are preferred instead of single phase ceria-based anodes. Ni, Ru, Pt and Pd are mainly proposed as metallic phase due to their catalytic activity in reforming reactions and C–H bond breaking. Ni-cermets attracted more interest due to their lower costs despite their promoting effect on carbon deposits formation.

Recently, Song et al. published a study of the electrocatalytic performance of $Ce_{1-x}Zr_xO_2$ ($x = 0.1, 0.25, 0.5, 0.75$ and 0.9) solid solutions as anode materials, by electrochemical impedance spectroscopy (EIS), in the symmetrical cell configuration [22]. Gadolinium doped ceria (GDC) was used as electrolyte and silver mesh, paint and wires were used as current collectors. All the solids were synthesized by citrate–nitrate combustion method. EIS experiments were performed in two humidified atmospheres: 5 vol.% H_2 (Argon balance) and 5 vol.% CH_4 (Argon balance). The authors observed a significant lower value of overall polarization resistance for $Ce_{1-x}Zr_xO_2$ ($x = 0.1, 0.25, 0.5, 0.75$) anode materials than that corresponding to pure ceria. On the contrary, the $Ce_{0.1}Zr_{0.9}O_2$ showed an inferior performance than CeO_2 when studied in the dilute methane atmosphere, and a similar one in the dilute hydrogen one. They found that the electrode compositions with the best electrochemical performance were those with the lower ZrO_2 contents: $Ce_{0.9}Zr_{0.1}O_2$ and $Ce_{0.75}Zr_{0.25}O_2$, which exhibited an excellent performance similar to that reported for GDC and SDC anodes in intermediate temperature SOFCs (IT-SOFCs).

In the present paper, we characterize the electrochemical behaviour of 60 wt.%NiO/$Ce_{0.9}Zr_{0.1}O_2$ cermets under different reducing atmospheres in symmetric cell configuration, [anode/electrolyte/anode]. SDC dense electrolytes were prepared from commercial CeO_2-10%mol Sm_2O_3 nanopowders. We also report the construction of button-type solid-oxide fuel cells with these materials and Pt as cathode. These cells were tested in pure and diluted hydrogen atmosphere at intermediate temperatures.

2. Experimental

2.1. Synthesis of powdered cermets

$Ce_{0.9}Zr_{0.1}O_2$ (hereinafter GS) mixed oxide was synthesized by the stoichiometric glycine/nitrate combustion route, previously reported [19]. After the synthesis process, the oxide was calcined at 600 °C in air in order to eliminate any vestige of carbonaceous residues. Negligible carbonaceous residues were observed after the calcination step through carbon elemental analysis. The mixed oxide exhibited fluorite structure with a high porous morphology, nanometric crystallite size and low agglomeration grade [19]. Nickel was incorporated by incipient wetness impregnation with $Ni(NO_3)_2 \cdot 6H_2O$ (99.8%, Baker Analyzed) ethanol solutions of suitable concentration, in order to form a final cermet with a NiO nominal content of 60 wt.%. In the reducing atmosphere of the anode chamber, NiO reduces to Ni°. In order to provide a good electronic conductivity, the Ni° content should be greater than ~ 30 vol.%. A Ni° content of 50 vol.% is generally preferred, which is equivalent to a 60 wt.% of NiO [23]. Therefore, this content was selected to assure a good electron percolation through the cermet. After impregnation, the solids were dried at 90 °C and calcined at 350 °C for 2 h in order to convert all the nickel compounds into NiO. This material will be referred hereafter as ZDC6.

2.2. Characterization of the powdered cermets

The texture, morphology and structure of ZDC6 powder were studied by N_2 Physisorption, Scanning Electron Microscopy (SEM) and X-ray Powder Diffraction (XPD) techniques, respectively.

Nitrogen adsorption isotherms at (-198 °C) were obtained in a Quantachrome Autosorb-1. Prior to the measurements, the samples were degassed at 250 °C for 7 h under vacuum (pressure < 20 μm Hg).

SEM micrographs were obtained with a Zeiss Electron Beam SEM-Supra 40. In order to avoid charging problems, the samples were placed over double-sided adhesive carbon-filled conductive ribbon.

XPD patterns were recorded with a Phillips PW3710 diffractometer using CuK_α radiation, equipped with a graphite monochromator and operated in a Bragg–Brentano configuration, at 40 kV and 30 mA. Data were collected in the $2\theta = 20-100°$ region, with a step-size of $0.02°$ and a step-counting time of 12 s.

2.3. Preparation of SDC electrolytes

Commercial powders of SDC (Samarium Doped Ceria-10% Sm_2O_3, Custom Material, Fuel Cells Materials) were uniaxially pressed at 1.5 ton cm^{-2}, and sintered at 1450 °C for 5 h with heating and cooling ramps of 5 °C min^{-1}. The diameter and thickness of the sintered disks were 16 mm and 0.7–1 mm, respectively, for the electrolytes used in symmetric cells, and 16 mm and 0.44 mm, respectively, for electrolyte disks used in the button-type SOFCs.

2.4. Assembly and evaluation of the symmetric [anode/electrolyte/anode] cells

The ZDC6 powder was mixed with a binder (Decoflux™ WB41, Zschiwmmer and Schwartz) in a 1:1 mass ratio, obtaining a slurry that was deposited on both sides of SDC sintered disks with a brush. The so-obtained symmetric cells were dried at 90–100 °C and sintered at three different temperatures for 2 h, 900 °C, 950 °C, and 1000 °C, in order to analyze the influence of sintering temperature on the polarization resistance of the anodes. Finally, to act as current collector, a very thin layer of Pt ink was deposited on the anode and fired at 900–950 °C for 30 min. The symmetrical cells were assembled into a lab-designed device that allows performing the experiments in different atmospheres.

The Electrochemical Impedance Spectroscopy (EIS) experiments were carried out in a Solartron 1260 frequency response analyser, with 20 mV of AC perturbation, in the 1 MHz to 0.01 Hz frequency domain. The impedance spectra were collected at isothermal

conditions, beginning at 800 °C and cooling down to 550 °C in 50 °C steps. At each temperature the dwell time was large enough to assure thermal stability and good repeatability. Feed gases were supplied at a constant flow of 40 cm^3 (STP) min^{-1}, and relative humidity of 3%. A small amount of water was added to the feed gases to avoid an excessive reducing atmosphere in the chamber, which could lead to excessive reduction of electrode and electrolyte materials leading to great volume expansion, crack formation and even delamination. Besides, the reduction of the SDC material of the electrolyte enhances its electronic conductivity resulting in a 'shortcut' of the cell, thus reducing its performance.

The feed compositions were 5 vol.% H$_2$ (N$_2$ balance) and pure H$_2$. All gas flows were monitored by mass-flow controllers.

The total electrode polarization resistance (R_p) was directly measured from the differences between the low and high frequency intercepts with the real axis on the impedance Nyquist curves. The area-specific resistance (ASR) of the electrode was calculated as: ASR $= 0.5 \cdot R_p \cdot A_e$, where A_e is the electrode area.

2.5. Preparation and evaluation of the button-type SOFCs

The ZDC6 as anode material and commercial Pt-ink as cathode material were fixed to the electrolyte following the same procedure described for the symmetric cell assembly at the optimal sintering temperature determined in the previous study using symmetric cells. The configuration of the cell was: ZDC6/SDC/Pt. These cells were tested in a homemade equipment, with pre-humidified 5 vol.% H$_2$ (N$_2$ balance) or pure hydrogen in the anode, and O$_2$ or synthetic air in the cathode. The measurements were performed at 600 °C and 650 °C. Simultaneously, the analysis of the electrochemical performance in the frequency domain was also carried out using a Solartron 1260 impedance/gain-phase analyser.

3. Results and discussion

3.1. Characterization of the ZDC6 powdered cermet

3.1.1. N$_2$ Physisorption

In Table 1 the BET specific surface area and total pore volume of the support and the cermet are presented. It is possible to see that there is a drop in total surface area and total pore volume of about 30%.

3.1.2. XPD analysis

Fig. 1 shows the XPD pattern of the sample ZDC6 after calcination at 1000 °C for 2 h in static air. The pattern exhibits the peaks of cubic fluorite-type crystal structure of Ce$_{0.9}$Zr$_{0.1}$O$_2$, superimposed with the NiO peaks, indicating that NiO appears as a separated phase.

No secondary phases or indications of compositional inhomogeneities were detected. Average crystallite sizes were calculated by the Scherrer equation, resulting of 38 nm for Ce$_{0.9}$Zr$_{0.1}$O$_2$ support and 78 nm for NiO.

3.1.3. SEM observations

A SEM micrograph of the ZDC6 powdered sample is shown in Fig. 2. It is possible to observe the NiO particles in the front plane and the smaller particles of the support in the back plane. Despite
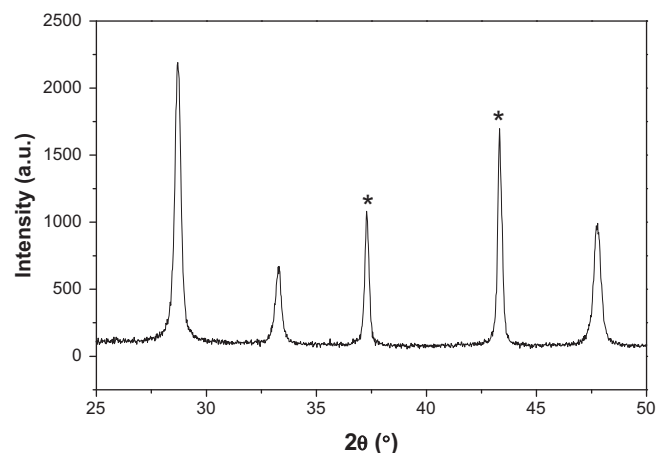
Table 1
BET specific surface area and pore volume of GS support and ZDC6 cermet.

Sample name	S_{BET} (m^2 g^{-1})	V_{pore} (cm^3 g^{-1})
GS	10	0.0091
ZDC6	7.2	0.0036

Fig. 1. XPD pattern of ZDC6 calcined at 1000 °C. "*" indicates the main peaks corresponding to NiO phase.

the high NiO content and calcination temperature used, it is possible to see in the micrographs the high porosity exhibited by the support, which favours the flow of gases through the anode. This observation is very important in thick-film anodes where the diffusion of the gas phase in the pores could be considered as an additional resistance affecting the global cell performance.

3.2. Symmetric [anode/electrolyte/anode] cells

3.2.1. SEM observations

A representative image of the constructed symmetric cells is shown in Fig. 3a and b, for the anode sintered at 1000 °C. It can be seen that the SDC electrolyte was dense (Fig. 3a), and the electrode has a porous structure even after the impregnation and sintering processes (Fig. 3b). The thickness of the anode was approximately 60−80 μm and its area was 0.2 cm^2. In Fig. 3a, a very thin layer of Pt contact, much less than 5 μm thick could be observed at the top of anode material.

3.2.2. Electrode performance

In order to select the optimal conditions to fix the anode, different sintering temperatures were selected and the corresponding electrochemical behaviour in diluted H$_2$ atmosphere was analyzed by EIS. In Fig. 4 it is possible to see the different ASR values
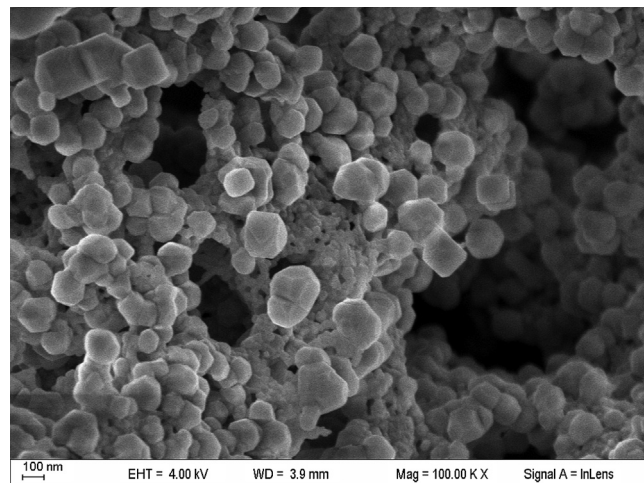

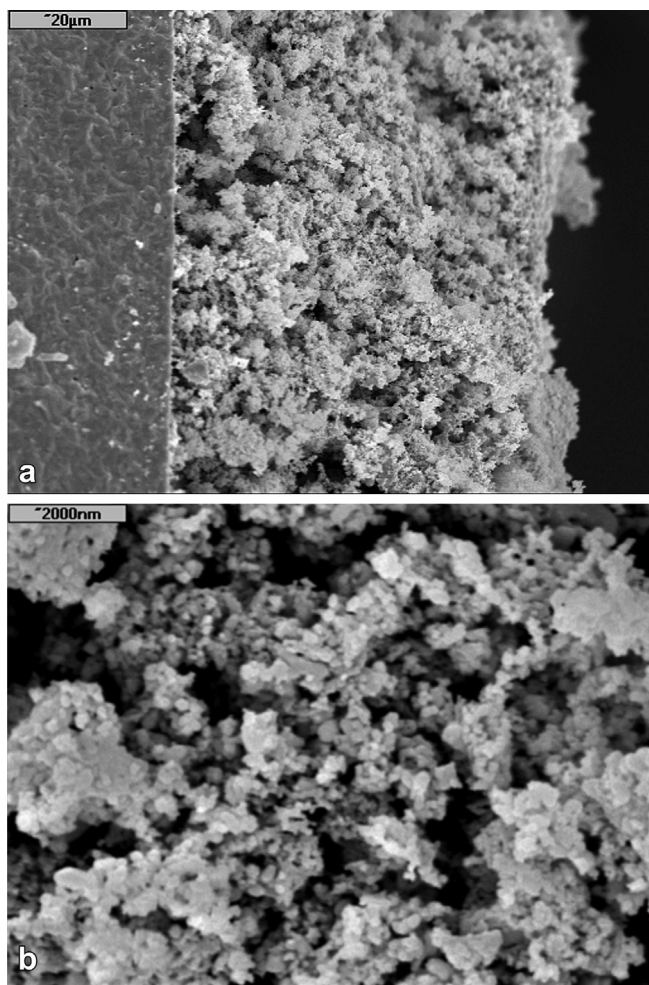**Fig. 2.** SEM micrograph of ZDC6 composite.

Fig. 3. SEM images of: (a) the electrolyte/anode interface; (b) the anode surface.

at different fixing temperatures, which lead to good adherence between anodic paint and electrolyte disk. Comparing the ASR values, it is clear that among the tested temperatures, the optimal sintering temperature is 1000 °C. In Fig. 5 the variation of ASR values with temperature is depicted.
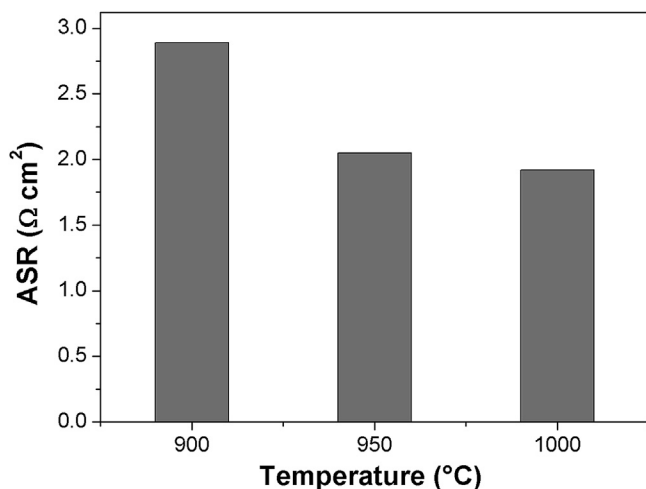

Fig. 4. ASR values obtained from experiments with symmetric cells tested at 550 °C in 5 vol.% H_2 (N_2 balance) gas-flow humidified with 3 vol.% H_2O, for different sintering temperatures.
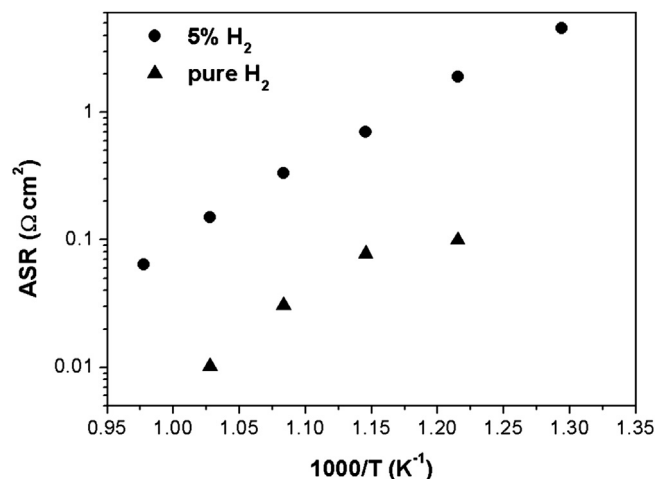

Fig. 5. ASR of the anode of this symmetric cell as a function of temperature for pure H_2 and diluted H_2 (5 vol.%).

After performing the experiments with a feed of 5 vol.% H_2 (N_2 balance), EIS measurements on pure H_2 were also performed in order to study the effect of the different atmospheres on the performance of the anode. These results are also depicted in Fig. 5. ASR values obtained at an operating temperature of 600 °C, with pure H_2 and diluted H_2 atmospheres, were 0.08 Ω cm^2 and 0.671 Ω cm^2, respectively. The best values reported in literature for conventional SDC anodes is 0.19 Ω cm^2 at 600 °C for pure H_2 [5], and 3.9 Ω cm^2 for $Ce_{0.9}Zr_{0.1}O_2$ anodes at 600 °C for diluted H_2 [22]. Therefore, our results demonstrate the excellent performance of the ZDC6 anode in both pure and diluted H_2 atmospheres. However, it is important to point out that the ASR values may be underestimated due to the contribution of electronic conductivity in ceria-based materials exposed to reducing atmospheres.

3.2.3. Modelling of electrochemical behaviour by equivalent circuits

The experimental data obtained from EIS experiments in symmetric cells were adjusted by equivalent circuits technique using ZView free-software from Scribner Associates, Inc. (version 2.9b), especially designed for EIS data analysis in electrochemical systems.

The models used to fit the impedance data are depicted in Fig. 6. Using both models, high quality fits with low relative errors were obtained. In both models, R_s represents the resistance induced by the electrolyte and all the external electronic resistances, as the platinum contacts, wires, etc. R_s can be displayed on the spectrum as the intersection of the impedance Nyquist diagram with the real axis in the high frequency region. The element R1-CPE fits the high frequency arc of the impedance spectrum [24]. To adjust the low frequency arc, two different elements were tested. In the first model (Fig. 6a: circuit N°1), a Warburg element was considered, while in the second one (Fig. 6b: circuit N°2) a Gerischer element was used. This low frequency arc is representative of the convolution of "non-charge transfer processes" like hydrogen exchange at surface, solid-state diffusion and gas-phase diffusion inside pores [25]. Warburg element is applicable when the process is controlled by solid-state diffusive mass transport [26]. Then, the Warburg element is used to model an anode behaviour where the diffusion of O^{2-} anions in the lattice of CeO_2–ZrO_2 mixed oxide is the main process. By using this adjustment it is possible to obtain the value of the ratio $L^2 \cdot D^{-1}$, where L is the effective diffusion length, and D the effective diffusion coefficient. On the other side, the Gerischer element (GE) has been used to model the behaviour of porous electrodes [22,27–29], involving diffusion processes coupled with
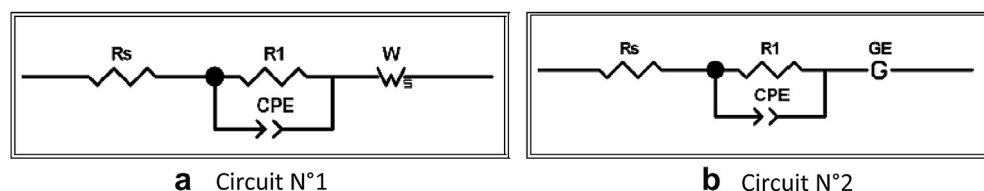
Fig. 6. Equivalent circuits used in the fitting of experimental EIS measurements.

chemical reactions. The Gerischer element is characterized by two parameters: an admittance parameter (Y_0 with units S s$^{1/2}$), and a rate constant (K_a, units of s^{-1}). In the high frequency edge, the Gerischer and Warburg elements are indistinguishable, since both elements have a frequency response showing a line at an angle of 45° respect to the real axis in the Nyquist plot, and a straight line of slope value of "$-1/2$" in the Bode plot.

In Fig. 7 the main parameters obtained from the fitting of EIS results in a 5 vol.% H_2 (N_2 balance) flow (40 cm^3 STP min^{-1}) are presented. In Fig. 7a the dependence of the effective diffusion time of the Warburg model with the temperature is plotted in an Arrhenius plot. It is possible to see that the plot is not linear; at high

Fig. 7. EIS fitting results of ZDC6 symmetrical cell, operated in 5 vol.% H_2 (N_2 balance) gas-flow humidified with 3 vol.% H_2O, using circuit N°1 (a) Variation of $L^2 \cdot D^{-1}$ parameter with temperature; (b) Variation of R_1 and W resistance values with temperature.

temperatures (between 700 and 800 °C), the slope of $L^2 \cdot D^{-1}$ is very pronounced, while below 700 °C there is a break in the slope. This observation is in agreement with the lower fitting quality obtained with equivalent circuit N°1 in comparison to that with circuit N°2. Nevertheless, some conclusions could be grasped from these results. It is observed a continuous decrease of the parameter $L^2 \cdot D^{-1}$ when the temperature is increased. This fact is an indication of the easier diffusion of O^{2-} ions into the ZDC6 structure at higher temperatures. From the values of parameter $L^2 \cdot D^{-1}$ it is possible to obtain the effective diffusion length of oxygen ions in the anode. Boukamp et al. [29], assuming a diffusion length in the order of the thickness of the active layer, obtained a D-value in the order of 10^{-6} cm^2 s^{-1}. Sameshima et al. [30] evaluated the oxygen ion diffusivities in $Ce_{0.8}R_{0.2}O_{1.9}$ mixed oxides (R = Yb, Y, Gd, Sm, Nd and La), from the electrical conductivity values obtained in experiments performed in dry air. For these materials, D values were in the range of 10^{-9}–10^{-7} cm^2 s^{-1}, in the temperature range of 400–800 °C, respectively. Taking into account the order of magnitude of these diffusivities for ceria-based mixed oxides, we obtained an effective diffusion length far below 80 μm, the normal thickness of the electrode material. Therefore, a reduction in the total impedance of the anode should be expected with the reduction of the thickness, when using another deposition technique like screen-printing.

In Fig. 7b the experimental data were also analyzed with the equivalent circuit N°2 (see Fig. 6b). The resulting values of parameters K_a and Y_0 are presented in the Arrhenius-type plot of Fig. 8. "K_a" represents the rate constant for the electrochemical reaction, and Y_0 is a parameter directly proportional to the concentration of diffusing species. From Fig. 8a it is clear that both parameters, Y_0 and K_a increase with the temperature with the corresponding decrease in the resistance of the G_E element. This behaviour is that expected for thermally activated processes with E_{Yo} = 97 kJ mol^{-1} and E_{Ka} = 27 kJ mol^{-1}. The activation energy for the rate constant is very low compared with the values found in the literature (50–120 kJ mol^{-1}) [22,28], indicating that this process has a low dependence with temperature. It can also be seen that the concentration of diffusing species into the anode (O^{2-}) increases with the temperature increment. This observation is in agreement with the results obtained from the fitting with the circuit 1, which indicates that at higher temperatures the diffusivity of oxygen ions is enhanced. The linearity observed in the Arrhenius plots obtained constitutes an indication that the fitting procedure carried out with circuit N°2 is reliable.

According to Boukamp et al. [28] the modelling with a Gerischer element is easily applicable to the case of diffusion processes coupled to chemical reaction and distributed charge-transfer steps. Besides, it is important to emphasize that for porous electrodes of mixed conductivity materials, like the one used in the present work, processes become even more complicated due to the presence of charge-transfer coupled with non-charge transfer processes distributed on the surface, pore gas-phase diffusion and redox processes.

As a supplementary analysis, the influence of the gas-flow fed to the cell was also studied. The impedance spectra obtained was adjusted using the two equivalent circuits previously presented
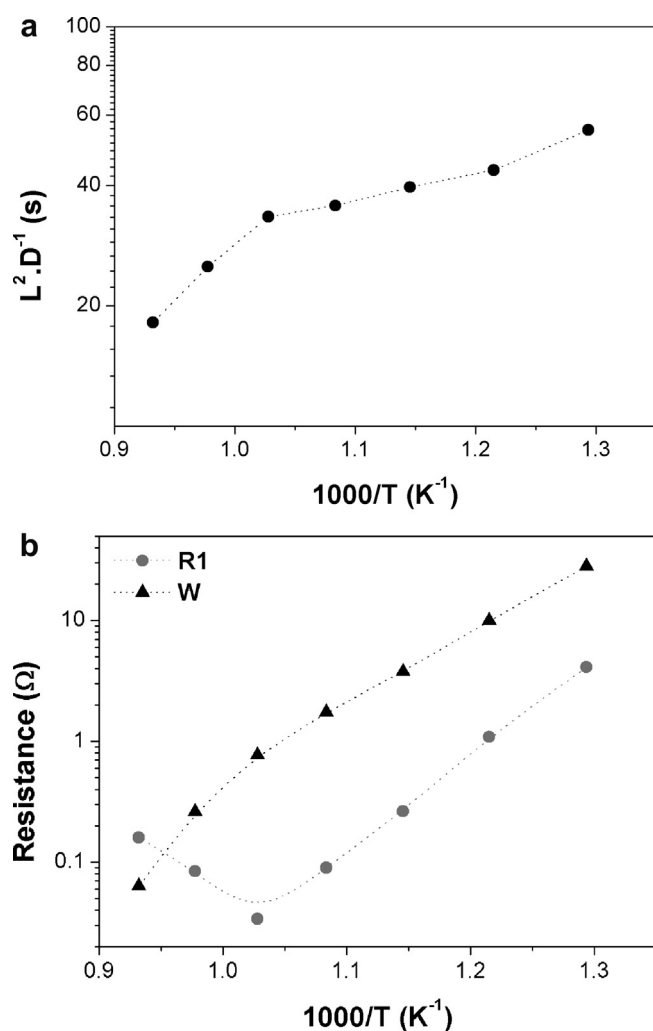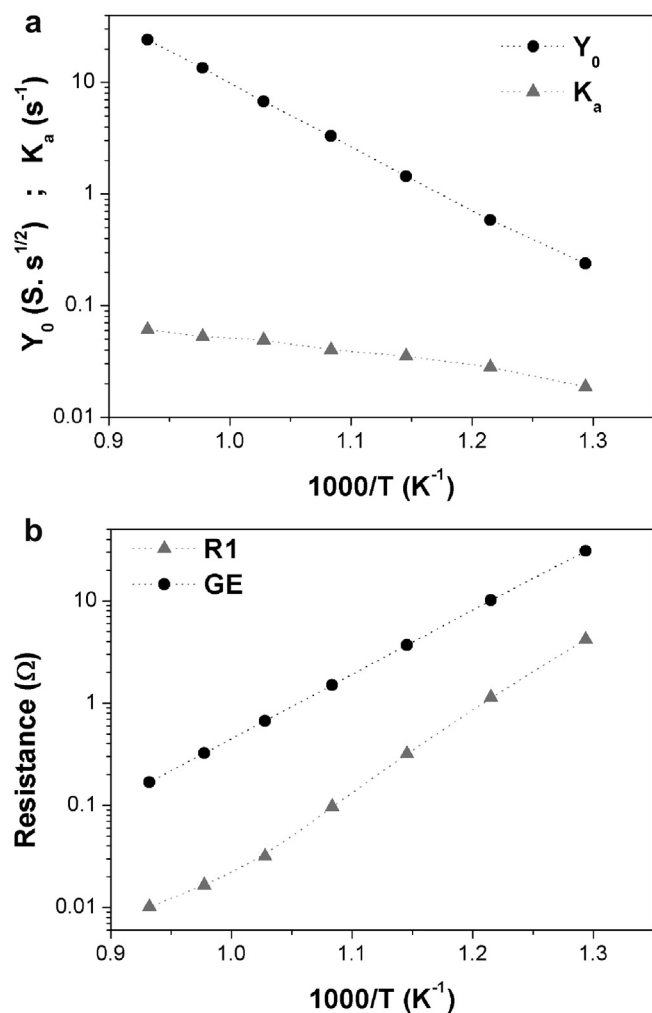
Fig. 8. EIS fitting results of ZDC6 symmetrical cell, operated in 5 vol%H_2 (N_2 balance) gas-flow humidified with 3 vol.% H_2O, using circuit N°2 (a) Variation of Y_0 and K_a parameters with temperature; (b) Variation of R_1 and G resistance values with temperature.

Fig. 9. EIS fitting results of ZDC6 symmetrical cell, operated in pure H_2 gas-flow humidified with 3 vol.% H_2O, using circuit N°2 (a) Variation of Y_0 and K_a parameters with temperature; (b) Variation of R_1 and G resistance values with temperature.

(Fig. 6). Values of gas-flow of 41, 82 and 105 cm³ STP min⁻¹ of 5 vol.% H_2 (N_2 balance) were tested. From the results obtained it is possible to conclude that the change in the gas-flow mainly influences the resistance value R1 associated with the oxidation of H_2 in anode/H_2 interface.

Impedance data of ZDC6 anode measured in symmetric cell configuration in pure H_2 at a flow rate of 41 cm³ STP min⁻¹ were also analyzed. In this case the equivalent circuit that provides the best fit of the experimental data was the circuit N°2, containing the Gerischer element. In Fig. 9 it is possible to see that, as in the case of 5 vol.% H_2 (N_2 balance) experiments, the resistances R_1 and G_E decrease as the temperature increases, and the parameter related to the concentration of oxygen ions increases. In this case, the rate constant K_a does not significantly change in the whole measured temperature range. Besides, the value of the resistance R_1 falls to zero at 700 °C. This is because at 700 °C, the high frequency arc in the impedance spectrum disappears, leaving only the impedance adjusted by Gerischer element. Therefore, the high frequency charge-transfer processes are not controlling the global process.

Song et al. [22] analyzed the impedance spectra of $Ce_{1-x}Zr_xO_2$ anode materials, under humidified 5% H_2 and humidified 5% CH_4, in terms of a double fractal finite length Gerischer impedance model. They found that Gerischer-type impedance dominates the
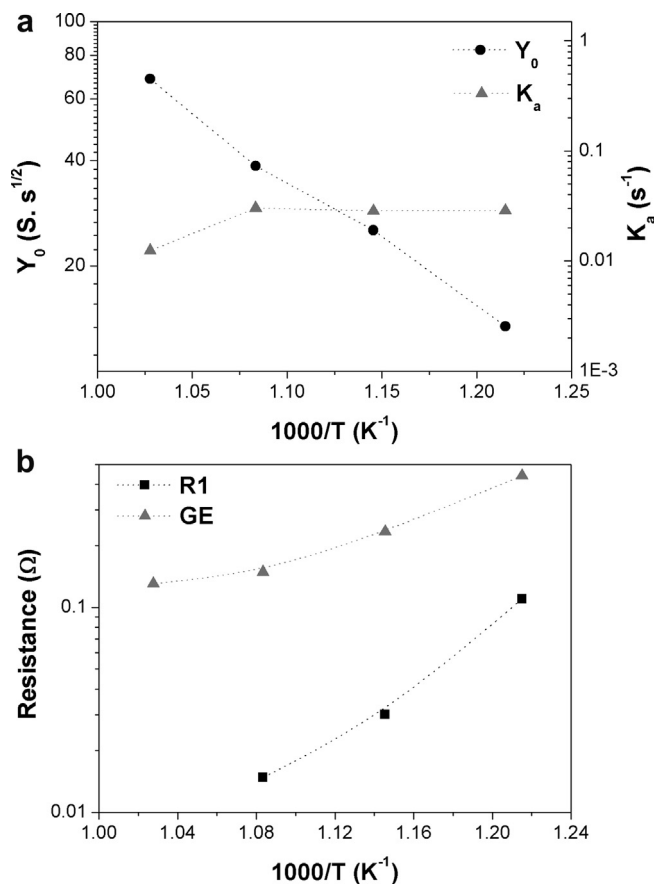
impedance spectra, masking the smaller feature associated with the electrochemical exchange reaction. In our case, this behaviour is only evident at high temperature in pure H_2 atmosphere.

3.3. Performance of the button-type SOFCs

In Fig. 10 the IV discharge curves and power density vs current density curves for ZDC6/SDC/Pt dual-chamber SOFCs, operated at different temperatures and gas-flow compositions, are presented. Besides, the Nyquist-plot of EIS measurements of the whole cell is shown in Fig. 11, at 600 °C, when pure H_2 is fed in the anodic chamber and O_2 or air are fed in the cathodic chamber.

Nernst theoretical potentials for the case of H_2/air atmospheres are 1.14 and 1.12 V, for 600 °C and 650 °C, respectively. The open circuit voltage (OCV) obtained in the experiments is lower than the corresponding Nernst potential. This phenomenon has been widely observed in SOFCs with ceria-based electrolytes. The explanation of this loss in OCV is that ceria-based electrolytes become n-type electronic conductors under reducing conditions. Then, the electronic conductivity of ceria under reducing conditions provides a path for electrons in the cell parallel to the external circuit producing a sharp drop on OCV [6].

Analyzing the discharge curve of Fig. 10, it is possible to observe an abrupt change in slope at 600 °C, when the current density exceeds the value of 0.18 A cm⁻², for oxygen-flow fed to the cathode, respectively. This abrupt change in slope at high current densities is generally associated with concentration polarization. That is, mass transfer problems arise at these current densities. This change in the slope is not detected in the measurement at 650 °C.
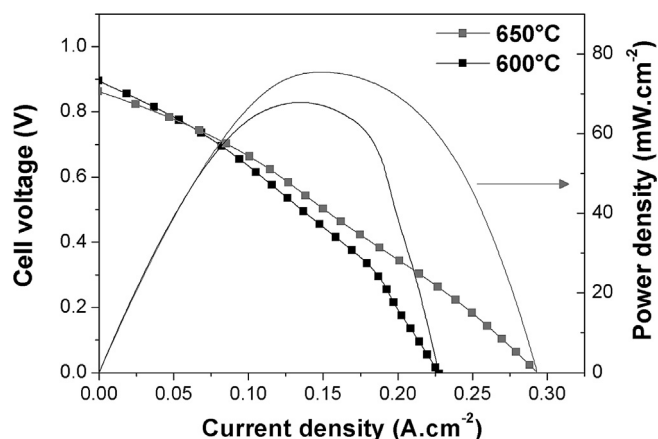
Fig. 10. IV-discharge curve for a ZDC6/SDC/Pt dual-chamber SOFC (temperatures: 600 and 650 °C). Fuel: Pure H_2 gas-flow humidified with 3 vol.% H_2O, oxidant: pure O_2.

The maximum power density obtained at 650 °C with pure and humidified hydrogen as fuel was 75 mW cm^{-2} when pure oxygen was fed to the cathodic chamber. These power density are higher than some values reported in the literature. In a recent work, Cela et al. [31] analyzed the performance of SOFCs prepared with NiO–$Ce_{0.9}Gd_{0.1}O_{1.95}$ anode, cathode of LSCF-SDC and YSZ electrolyte. At
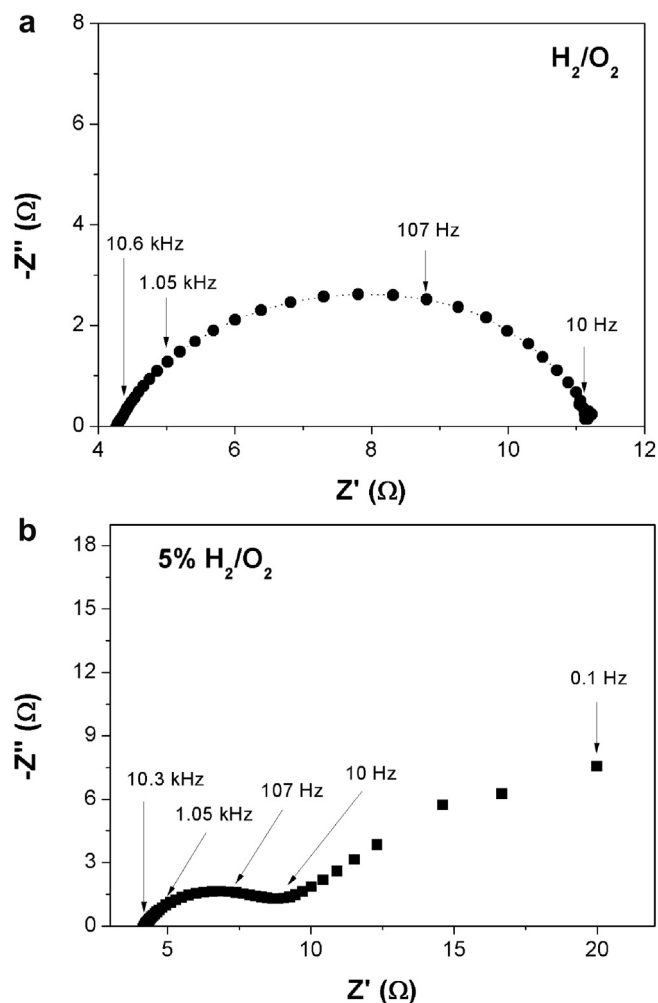

Fig. 11. Nyquist-plot for a ZDC6/SDC/Pt dual-chamber SOFC at 600 °C under: (a) Fuel: pure H_2 gas-flow humidified with 3 vol.% H_2O; oxidant: pure O_2; (b) Fuel: 5 vol%H_2 (N_2 balance) gas-flow humidified with 3 vol.% H_2O; oxidant: Pure O_2.

850 °C it is achieved a maximum power density of about 55 mW cm^{-2}, feeding dry H_2 as fuel and oxygen as oxidant. Nevertheless, it is important to note that power densities far above these values are found in the literature. He et al. [32] reported maximum power densities of 450 and 350 mW cm^{-2} at 600 °C, with pure and humidified hydrogen as fuel, for cells made of NiO–CeO_2/SDC/SSC and NiO–CeO_2–Gd_2O_3/SDC/SSC, respectively. However, it is important to remark that these high values of power densities were obtained with an electrolyte thickness (30 μm) much smaller than the thickness of our electrolyte disks (400 μm). Another important point is that in our work, the material used in the cathode was just a commercial Pt ink, which is not efficient enough in the oxygen exchange process, leading to lower power densities.

Fig. 11 shows the impedance of the cell at 600 °C, when pure and diluted hydrogen is fed at the anode, and oxygen at the cathode. It can be seen the variation of the polarization resistance when the fuel is changed from pure to diluted hydrogen. ASR values of the cell are 1.64 and 9.34 Ω cm^2 for pure H_2 and 5 vol.% H_2 (N_2 balance), respectively. In the Nyquist plot it is possible to see only one semicircle when the cell is operated with pure H_2 in the anodic chamber, and two semicircles when the cell is operated with diluted H_2. The same behaviour was observed in the EIS experiments performed with symmetric cells. Therefore, it is evident that with pure H_2 as fuel the charge-transfer processes at interfaces (electron transfer at current-collector/electrode and ions transfer at electrode/electrolyte interfaces) are very fast.

4. Conclusions

This paper presents the electrocatalytic performance of 60%NiO/$Ce_{0.9}Zr_{0.1}O_2$ (ZDC6) anode nanomaterial obtained by glycine-nitrate gel-combustion process. The Electrochemical Impedance Spectroscopy (EIS) test performed under reducing atmospheres, using a symmetric cell configuration, [anode/electrolyte/anode], with Samaria doped Ceria (SDC) as electrolyte, allowed finding that 1000 °C was the better temperature to fix the ZDC6 material onto the SDC sintered discs among the three fixing temperatures used. Even though the fixing temperature is quite high, it was observed on SEM micrographs that the anode material retains a high porosity. Excellent ASR values were obtained, showing that the ZDC6 anode exhibits excellent performance compared to conventional anodes reported in the literature.

Electrochemical impedance spectroscopy results performed on symmetrical cells allowed obtaining important information about the behaviour of the anode material. The impedance spectra were fitted with two models, one considering a Warburg element and the other a Gerischer element for the fitting of the low frequency arc. High quality fittings were obtained with both models. Nevertheless, the second model with a Gerischer element was better. The model parameters indicated that the effective diffusion length is far below the thickness of the anode. This fact suggests that a better performance could be achieved by reducing the anode thickness. The charge-transfer processes at interfaces are fast and their contribution to total impedance is only evident in diluted hydrogen experiments. The impedance spectrum is dominated by the low frequency arc. It was also concluded that changes in the gas-flow mainly influences the resistance associated with the oxidation of hydrogen at $H_2(g)$/anode interface.

Button-type SOFCs prepared with ZDC6 anode, SDC as electrolyte and commercial Pt-ink as cathode, were successfully tested. Different anodic and cathodic atmospheres were evaluated. Good power densities were achieved at intermediate temperatures (600 and 650 °C), taking into account that the cathode used in this work has a poor performance in the oxygen reducing reaction. The present results indicate that 60%NiO/$Ce_{0.9}Zr_{0.1}O_2$ cermet is a very

promising anode material for its use in IT-SOFCs operated under H_2 atmospheres.

Acknowledgements

References

[1] A.J. Jacobson, Chem. Mater. 22 (2010) 660–674.
[2] S. MacIntosh, R. Gorte, Chem. Rev. 104 (2004) 4845–4865.
[3] R.J. Gorte, J.M. Vohs, S. McIntosh, Solid State Ionics 175 (2004) 1–6.
[4] R.J. Gorte, H. Kim, J.M. Vohs, J. Power Sources 106 (2002) 10–15.
[5] J.W. Fergus, Solid State Ionics 177 (2006) 1529–1541.
[6] C. Sun, U. Stimming, J. Power Sources 171 (2007) 247–260.
[7] W. Zhu, S. Deevi, Mater. Sci. Eng. A362 (2003) 228–239.
[8] O.A. Marina, M. Mogensen, Appl. Catal. A 189 (1999) 117–126.
[9] www.fuelcellmaterials.com, Document N°11-002.
[10] C. Lu, W.L. Worrell, C. Wang, S. Park, H. Kim, J.M. Vohs, R.J. Gorte, Solid State Ionics 152–153 (2002) 393–397.
[11] O.A. Marina, C. Bagger, S. Primdahl, M. Mogensen, Solid State Ionics 123 (1999) 199–208.
[12] C. Xia, M. Liu, Solid State Ionics 144 (3–4) (2001) 249–255.
[13] D.G. Ivey, E. Brightman, N. Brandon, J. Power Sources 195 (2010) 6301–6311.
[14] M. Chen, B.H. Kim, Q. Xu, O.J. Nam, J.H. Ko, J. Eur. Ceram. Soc. 28 (2008) 2947–2953.
[15] G. Meng, C. Jiang, J. Ma, Q. Ma, X. Liu, J. Power Sources 173 (2007) 189–193.
[16] S. Larrondo, M.A. Vidal, B. Irigoyen, A.F. Craievich, D.G. Lamas, I.O. Fábregas, G.E. Lascalea, N.E. Walsöe de Reca, N. Amadeo, Catal. Today 107–108 (2005) 53–59.
[17] S. Pengpanich, V. Meeyoo, T. Rirksomboon, K. Bunyakiat, Appl. Catal. A 234 (2002) 221–233.
[18] C. Bozo, N. Guilhaume, E. Garbowski, M. Primet, Catal. Today 59 (2000) 33–45.
[19] M.G. Zimicz, I.O. Fábregas, D.G. Lamas, S.A. Larrondo, Mat. Res. Bull. 46 (2011) 850–857.
[20] M.G. Zimicz, D.G. Lamas, S.A. Larrondo, Catal. Commun. 15 (2011) 68–73.
[21] M.G. Zimicz, S.A. Larrondo, R.J. Prado, D.G. Lamas, Int. J. Hydrogen Energy 37 (19) (2012) 14881–14886.
[22] S. Song, R.O. Fuentes, R.T. Baker, J. Mater. Chem. 20 (2010) 9760–9769.
[23] J.C. Ruiz Morales, et al., in: Centro de la Cultura Popular Canaria (Ed.), Pilas de combustible de óxidos sólidos: SOFC (2008), ISBN 978-84-7926-567-0. Tenerife, España.
[24] S.B. Adler, Solid State Ionics 135 (2000) 603–612.
[25] B.A. Boukamp, H.J. Bouwmeester, Solid State Ionics 157 (2003) 29–33.
[26] J.R. Macdonald, E. Barsoukov, Impedance Spectroscopy: Theory, Experiments and Applications, Wiley-Interscience, John Wiley & Sons, Inc., 2005.
[27] M. González-Cuenca, W. Zipprich, B.A. Boukamp, G. Pudmich, F. Tietz, Fuel Cells 1 (3–4) (2001) 256–264.
[28] B.A. Boukamp, M. Verbraeken, D. Blank, P. Holtappels, Solid State Ionics 177 (2006) 2539–2541.
[29] B.A. Boukamp, Solid State Ionics 136–137 (2000) 75–82.
[30] S. Sameshima, H. Ono, K. Higashi, K. Sonoda, Y. Hirata, Y. Iruma, J. Ceramic Soc. Jpn. 108 (12) (2000) 1060–1066.
[31] B. Cela, D.A. de Macedo, G. de Souza, A. Martinelli, R. do Nascimento, C. Paskocimas, J. Power Sources 196 (5) (2011) 2539–2544.
[32] B. He, D. Ding, C. Xia, J. Power Sources 195 (2010) 1359–1364.